EXTENDING THE ECOB SPACE DEBRIS INDEX WITH FRAGMENTATION RISK ESTIMATION

F. Letizia[1], C. Colombo[2], H. G. Lewis[3], and H. Krag[4]

[1] *University of Southampton, SO17 1BJ Southampton, United Kingdom, Email: f.letizia@soton.ac.uk*
[2] *Politecnico di Milano, 20156 Milan, Italy, Email: camilla.colombo@polimi.it*
[3] *University of Southampton, SO17 1BJ Southampton, United Kingdom, Email: h.g.lewis@soton.ac.uk*
[4] *European Space Agency, 64293 Darmstadt, Germany, E-mail: Holger.Krag@esa.int*

ABSTRACT

In recent years several formulations of debris indices have been proposed to provide a fast assessment of the criticality of a space object in terms of its impact on the debris environment. In a previous work, we proposed a formulation (ECOB, Environmental Consequences of Orbital Breakups) based on the evaluation of the consequences of the fragmentation of the studied object in terms of the increase in the collision probability for operational satellites. This work discusses the extension of that approach by considering not only the effect of the fragmentation but also its likelihood. In addition, a method to take into account different End-of-Life scenarios and the application to constellations are discussed.

Key words: debris index; debris clouds.

1. INTRODUCTION

Several authors have highlighted the relevance of having a quantitative measure of the vulnerability of an object in orbit and of its effects on the space debris environment [13, 20, 17, 3, 12, 15, 16, 2, 1]. The proposed debris indices focus on different aspects of the debris environment, ranging from the likelihood that a space object will be involved in a collision with a piece of debris to the evaluation of the long-term changes in the whole debris population. In addition, some of the previous studies [20, 17, 16, 1] have proposed analytical formulations for their indices, which can be immediately computed and offer a fast assessment of the criticality of a space object without requiring access to extensive computational resources or to evolutionary debris models. These approaches are particularly interesting as they open the way for debris indices to become a tool for operators, analysts, regulators to support the preliminary analysis of a mission, the evaluation of the compliance with space debris guidelines and the identification of the most critical elements in the population. This last aspect can also be exploited to design active debris removal missions.

In a past work [10] we proposed a debris index that does not have such an analytical formulation, but still allows for a fast analysis as the results that depend on the simulation of the debris evolution are conveniently stored in maps that can be accessed to perform the actual computation of the index. The proposed index, called ECOB (Environmental Consequences of Orbital Breakups), as the name suggests, focussed on the evolution of the consequences (i.e. the effects) of a fragmentation. In particular, the fragmentation of the studied object was simulated and its effect was measured in terms of the resulting collision probability for a set of targets representative of the operational satellites in the considered portion (700-1000 km) of the Low-Earth Orbit (LEO). The representative targets are defined by applying a grid on the studied orbital region (Fig. **??**) and identifying a representative target for the cells with the highest cumulative cross-sectional area, until a fixed ratio of the total cross-sectional area (e.g. 0.9) is considered.

The index is defined as

$$\text{ECOB} = \sum_{j=1}^{N_T} w_j p_{c,j}, \tag{1}$$

where $p_{c,j}$ is the cumulative collision probability for each representative target and w_j a weighting factor to give more importance to targets that represent orbital regions containing a high cumulative cross-sectional area (Fig. 1).

Instead of computing the index only for specific objects, a grid in semi-major axis and inclination was introduced to define a large array of possible orbital conditions of catastrophic collisions, i.e. collisions where the whole object fragments. The corresponding value of ECOB, for a fixed value of the object mass (10 000 kg), is computed and stored in a *map*. The value of the index for a different mass can be obtained by a simple rescaling

$$\text{ECOB}(M) = \text{ECOB}(M_{10\,000\,\text{kg}})\Big(\frac{M}{10\,000\,\text{kg}}\Big)^{0.75}. \tag{2}$$

In this way, as anticipated, once the *map* is generated ECOB can be computed immediately for any object by

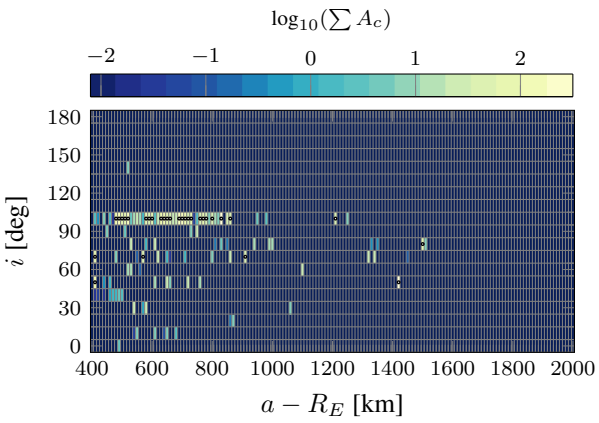

Figure 1. Distribution of the cross-sectional area of spacecraft launched in the last 10 years, in orbit between 400 and 2000 km.

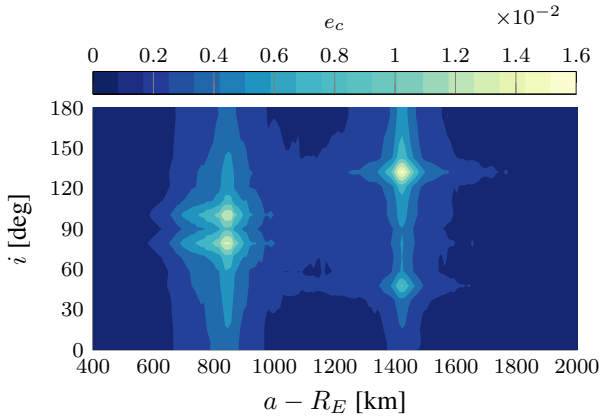

Figure 2. Variation of the term e_c with the orbital parameters.

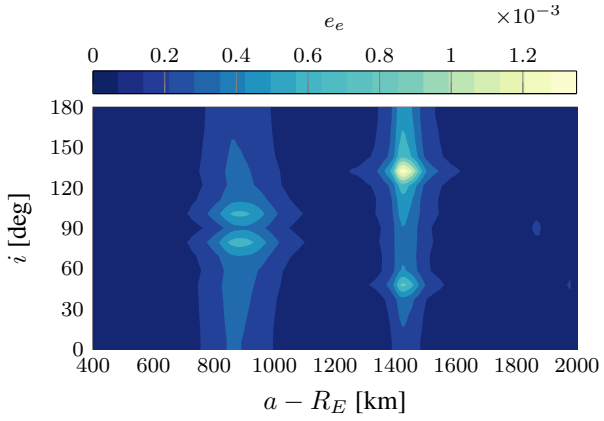

Figure 3. Variation of the term e_e with the orbital parameters.

rescaling and interpolating the values in the map considering the specific parameters of the object (i.e. semi-major axis, inclination, mass).

2. FORMULATION OF THE DEBRIS INDEX

The ECOB index described in [10] has been enhanced by extending its applicability region, including more factors in its formulation, devising a method to take into account different mission profiles, and including the possibility of dealing with constellations.

First, the propagation method for the debris cloud was changed so that the limits on the applicability only to 700-1000 km is not present anymore. As a result, now the index can be computed for any object between 400 and 2000 km. Further details on the propagation method and on its validation can be found in [9].

A second point of improvement is the extension of the index formulation to take into account not only the effect of fragmentations, but also their likelihood. More in the details, the suggested formulation becomes now

$$I = p_e \cdot e_e + p_c \cdot e_c, \tag{3}$$

where the e terms refer to *effects*. Exactly like for ECOB, these terms measure the effect of a fragmentation by looking at the increase in the collision probability for a set of reference targets. While ECOB models only the fragmentation clouds generated by catastrophic collisions, the new index (I) in Eq. 3 models also fragment clouds generated by explosions (e_e, whereas e_c is ECOB). As for ECOB, these terms are not simply computed for specific objects, but rather evaluated on a grid of semi-major axis and inclination. The results for the two terms are shown in Figures 2 and 3. Also for the case of explosions, a dependence on the mass is introduced even if not explicitly present in the breakup model used for the generation of the debris clouds. A linear relationship between the mass and the number of generated fragments is used [11].

In Eq. 3 the p terms refer to probabilities. For the case of collisions, p_c is obtained from the analogy with the kinetic theory of gas, so that

$$p_c = 1 - \exp\left(-\rho \Delta V A \Delta t\right) \tag{4}$$

where ρ is the density of debris objects large enough to trigger a catastrophic collision, ΔV is the impact velocity, A is the object cross-sectional area and Δt is the selected time period (e.g. one year). Both ρ and ΔV are obtained from ESA MASTER, considering the debris population at a specific epoch. For ρ, it is possible to specify if the object is active and in that case the debris objects larger than 10 cm are not included in ρ, assuming that they can be avoided with manoeuvres. However, this is an optimistic assumption as also the information on the actual orbit control capability of the object would be needed. In any case, it was observed that the inclusion or exclusion of debris objects larger than 10 cm affects the final value of the index in a minor way (less than 5%) for

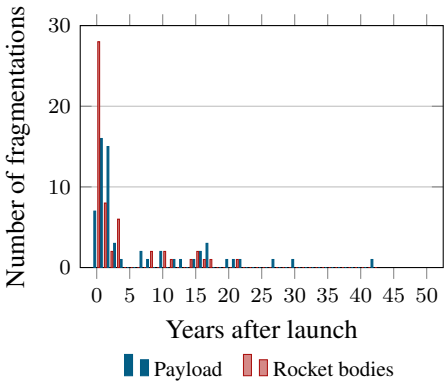

Figure 4. Distribution of the explosion events as a function of the elapsed time since the launch.

typical objects in Sun-synchronous orbit. All the results in the following are obtained always including also objects larger than 10 cm. Also for ΔV a grid in semi-major axis and inclination is defined; for each orbit, MASTER is used to obtain the most probable impact velocity derived from the flux distribution.

Finally, the term p_e is obtained from the data on historical fragmentations available in DISCOS (Database and Information System Characterising Objects in Space)[1] [5]. The data was filtered considering fragmentation events only happened in LEO, involving objects launched after 1985 and whose fragmentation is due to battery or propulsion failures, or unknown causes. Fig. 4 shows the distribution of the number of events as a function of the years elapsed between the launch and the event, distinguishing between payloads and rocket bodies. The distribution shows clearly that most events occurred in the first years, with only a few events happening after 20 years or later. This distribution appears quite stable for objects launched in different epochs, so a first estimation of the probability of explosion can simply be obtained by normalising the number of events in Fig. 4 with the number of objects launched in the same time period.

3. FROM EFFECTS TO RISK

This section analyses more in detail the terms of the index relative to collisions

$$I_c = p_c \cdot e_c \tag{5}$$

to understand how the addition of the term p_c affects the results already obtained for e_c presented in [10]. To facilitate the comparison with the previous results, only the region between 700 and 1000 km is considered here.

The first analysis is based on considering a cases with fixed mass (10 000 kg) and looking only at the variation with semi-major axis and inclination. For the effect of a

[1] Accessible at `https://discosweb.esoc.esa.int/`.

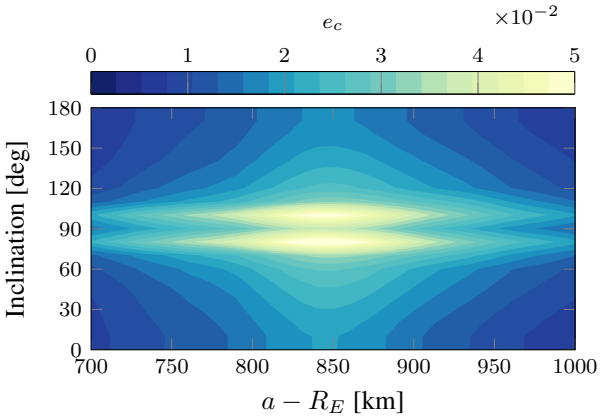

Figure 5. Variation of the term e_c with the orbital parameters [10].

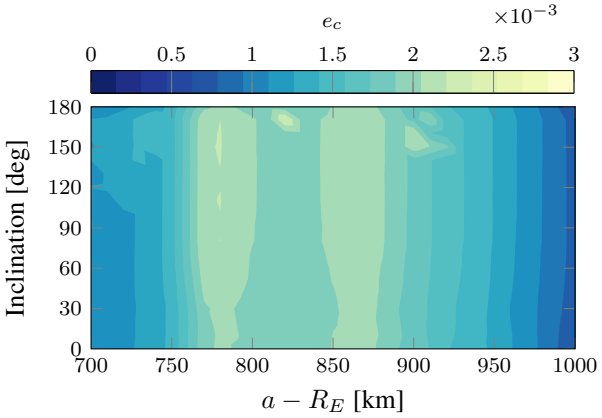

Figure 6. Variation of the term p_c with the orbital parameters.

fragmentation generated by a collision, the map in Fig. 5 was found in [10].

Similar maps were generated to study the variation of p_c (Fig. 6) and I_c (Fig. 7). For what concerns p_c, its variation is dominated by the one of the debris density ρ as it can be observed by the two peaks around 780 km and 860 km that come from the distribution of the background debris density. The impact velocity has instead a more limited variation, ranging between 11.5 km s^{-1} and 14.5 km s^{-1} across the domain. The distribution of the velocity is responsible for the local increase of the collision probability at inclinations around 150°.

Looking at the distribution of I_c in Fig. 7 one can still recognise the pattern coming from the variation of e_c because of the location of operational satellites; the effect of p_c is to distort the distribution of e_c to take into account also the distribution of the debris population by increasing the value of the index at the altitudes around 780 km and 860 km.

Another possible analysis is to study the dependence of

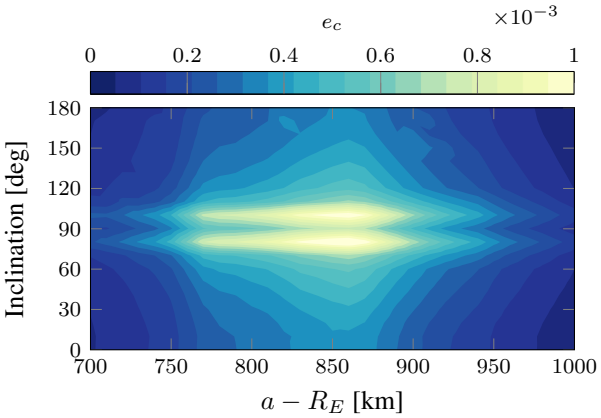

Figure 7. Variation of I_c with the orbital parameters.

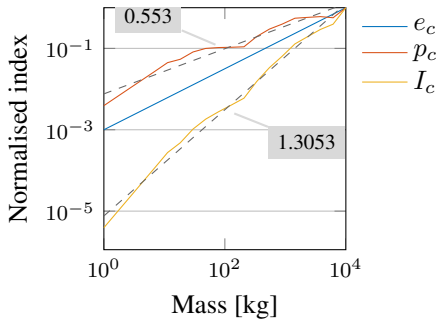

Figure 8. Variation of e_c, p_c, I_c with the mass. Indices normalised with the value at $m = 10\,000$ kg and computed for object in orbit at 850 km of altitude, on an orbit with inclination equal to 98°. The numbers in grey refer to the exponent of the closest approximation with a power law.

the indicators (e_c, p_c, I_c) on the mass as shown in Fig. 8. For e_c it was already found that the dependence on the mass is described by a power law with exponent equal to 0.75 as a consequence of the equations in the breakup model [7]. In the case of p_c, the variation with the mass is driven by two factors. Recalling the equation

$$p_c = 1 - \exp\left(\rho \Delta v A_c \Delta t\right),$$

the two terms affect by the mass the debris density ρ and the cross-sectional area A_c. In the first case, ρ, which indicates the density of objects able to trigger a catastrophic collision, decreases if the mass increases; on the other hand, A_c grows linearly with the mass because a constant area-to-mass ratio is used. The combined effect leads still to an increase of p_c with the mass, but with a less steep curve than for e_c. Fig. 8 shows an approximation of p_c with a power law (with coefficient of determination R^2 equal to 0.9585) with exponent equal to 0.553. As the global index I_c is obtained from the multiplication of e_c and p_c, it also increases with the mass. In this case the approximation with a power law ($R^2 = 0.9922$) presents exponent equal to 1.3.

A final test was performed by computing the index for the objects in the DISCOS database and looking at which are the ten objects with the highest values of e_c and I_c. The detailed parameters of all the objects are listed in Tab. 1. For this analysis, the actual cross-sectional area of the object is considered, differently from what shown in [10].

One can observe how with I_c all the objects belong to the peak areas with at altitudes between 760 and 870 km. In particular, Cosmos 2502 and 2455, both in an orbit at 905 km of altitude, are not any longer in the top ten objects when I_c is considered instead of e_c because that orbital region is less critical in terms of background debris population. Similarly for Cosmos 2486 and 2441, in orbit at 720 km of altitude, that are in the top ten when only the effects of a fragmentation are considered, but ranks over the 120th place when also the collision probability is taken into account. The first object is the same (Envisat) with both classifications, whereas one can observe how objects with a large area-to-mass ratio (A/M) have a large collision probability and so they rank higher in the collision risk index.

4. DISPOSAL OPTIONS

The proposed structure of the index still does not capture one aspect that may be relevant if the debris index is used for an evaluation of the sustainability of a space mission. This aspect is the implementation of disposal strategies at the end of a mission. Eq. 3 provides a snapshot of a specific condition of a spacecraft, so a way to take into consideration different disposal actions is to compute the index in Eq. 3 at different time steps along the mission profiles, following the approach suggested by Yasaka [20] for his formulation of a debris index.

When a disposal strategy is implemented, the spacecraft leaves its slot at the end of the mission and it is either moved towards higher altitudes or towards the Earth to re-enter in the atmosphere and burn up. Three main options for the disposal are considered: 1) no disposal, when the spacecraft is left uncontrolled on the operational orbit; 2) re-orbit, when the spacecraft is moved to an orbit different from the operational one; 3) de-orbit, when the spacecraft re-enters in the atmosphere. Fig. 9 shows a schematic example of the evaluation of the index along the mission profiles for three possible disposal strategies. For simplicity, it is assumed that the operational orbit has a debris index ten times larger than any other orbit. In the first case, no disposal is performed, so the level of the debris index stays constant indefinitely. In the second case, the spacecraft is re-orbited to a less critical region. In the last case, a disposal strategy compatible with current guidelines [4] is implemented and the spacecraft is de-orbited to a lower altitude, from where it re-enters in the Earth atmosphere within 25 years from the end of its mission.

These three scenarios can be compared by looking at the area enclosed by each profile in Fig. 9. This analysis is of course affected by the time-window considered as shown

Table 1. Top ten payloads with highest I_c or e_c.

SATNO	Name	$a - R_E$ [km]	i [°]	m [kg]	A [m^2]	A/M [m^2/kg]	p_c	e_c	I_c	Rank e_c	Rank I_c
27386	Envisat	772.7	98.27	8110	74.3903	0.009173	0.026488	0.029847	7.91E-04	1	1
27597	Midori-2	808.1	98.34	3680	55.5507	0.015095	0.029961	0.020366	6.10E-04	4	2
22823	SPOT 3	835.4	98.91	1891	27.7663	0.014684	0.034683	0.014246	4.94E-04	42	3
24277	Midori	801.0	98.69	2469	42.9907	0.017414	0.033777	0.014568	4.92E-04	40	4
38771	Metop-B	827.5	98.72	4086	37.4921	0.009176	0.017894	0.024569	4.40E-04	2	5
29499	Metop-A	827.5	98.72	4086	37.4921	0.009176	0.017893	0.024567	4.40E-04	3	6
40069	Meteor-M No. 2	830.3	98.69	2755	26.7438	0.009707	0.019575	0.018495	3.62E-04	11	7
35865	Meteor-M No. 1	825.5	98.45	2755	26.7438	0.009707	0.019322	0.018013	3.48E-04	12	8
40336	CBERS 4	780.7	98.48	2100	22.1961	0.010570	0.030623	0.011322	3.47E-04	61	9
20322	COBE	884.4	98.97	2245	19.5988	0.008731	0.023051	0.014249	3.28E-04	41	10
33272	Cosmos-2441	727.2	97.95	7000	16.2224	0.002317	0.002851	0.019952	5.69E-05	5	121
11165	Cosmos-1066	861.2	81.24	2725	5.8996	0.002165	0.004664	0.019349	9.02E-05	6	75
40699	Cosmos-2506	722.1	98.24	7000	16.2224	0.002317	0.002779	0.019165	5.33E-05	7	126
39177	Cosmos-2486	722.2	98.18	7000	16.2224	0.002317	0.002781	0.019163	5.33E-05	8	125
36095	Cosmos-2455	912.3	67.15	7000	16.2224	0.002317	0.004255	0.018824	8.01E-05	9	87
40358	Cosmos-2502	912.5	67.15	7000	16.2224	0.002317	0.004251	0.018812	8.00E-05	10	88

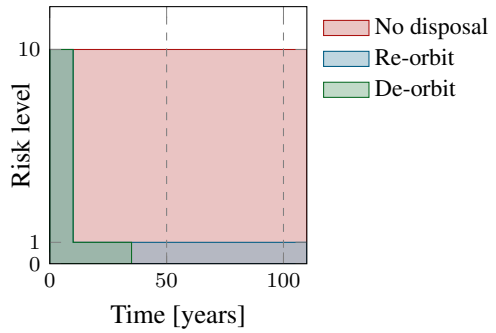

Figure 9. Debris index for different disposal profiles as a function of the years after launch.

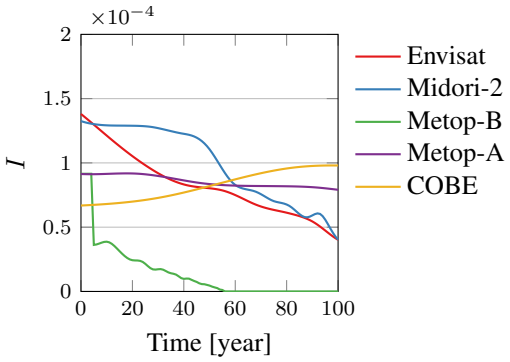

Figure 10. Debris index for different objects in the DISCOS population assuming de-orbit for active spacecraft (in orbit for 10 years or less).

Table 2. Example of index computation for the missions profiles in Fig. 9 and two different time-windows of, respectively, 50 and 100 years. The number between bracket indicates the relative value compare to the no-disposal option.

	50	100
No disposal	500 (1)	1000 (1)
Re-orbit	140 (0.28)	190 (0.19)
De-orbit	125 (0.25)	125 (0.125)

with an example in Tab. 2. The choice of the time window should be carefully selected and tested to ensure that the debris index is able to distinguish among the three options, while keeping a good balance between short and long term effect of space debris. A time window of 100 years was selected. This time period make it possible to distinguish among objects left in orbits with different altitudes (e.g. at $600\,\mathrm{km}$ or at $800\,\mathrm{km}$). In addition, the selected period is long enough to penalise in a clear way missions that do not perform a disposal.

The mission profile can be provided as input to the computation of the index, giving the variation of semi-major axis and inclination over the selected time window. Alternatively, one can define some standard strategies: this approach can be useful when one wants to compare many objects within a given population. For example, focussing on the objects with semi-major axis larger than $700\,\mathrm{km}$, one possible disposal option is that active spacecraft are moved to an orbit with altitude equal to $600\,\mathrm{km}$, from where the natural re-entry intro the Earth atmosphere takes around 20 years for a spacecraft with area-to-mass ratio $A/M = 0.006\,\mathrm{m^2\,kg^{-1}}$, which is the average value found among the operational spacecraft in orbit between 700 and $1000\,\mathrm{km}$ of altitude. For all objects except active spacecraft the trajectory is propagated over the selected time span (e.g. 100 years); the trajectory is then sampled at a constant rate (e.g. one year) and the index I in Eq. 3 is computed at each time step. In this way, profiles such as the ones in Fig. 10 are obtained. For active spacecraft, the parameters are kept constant for the period when the spacecraft is operational (e.g. ten years) and then the trajectory is integrated using the initial conditions appropriated for the selected de-orbiting altitude (e.g. $600\,\mathrm{km}$ as mentioned above).

Fig. 10 was generated using the data from DISCOS and assuming that payloads in orbit since ten years or less are still active and so they can perform a disposal manoeuvre. This is the case, for example, for Metop-B, whereas all

Table 3. Objects with the highest value of I and of the cumulative index computed along the mission profile ($\int I\,\mathrm{d}t$).

ID	SATNO	Name	Year	Disposal	$\bar{h}$ [km]	i [°]	m [kg]	I	$\int I\,\mathrm{d}t$	Rank I	Rank $\int I\,\mathrm{d}t$
29	27386	Envisat	2002	No	770.8	98.45	8110	0.000159	0.008365	1	3
92	27597	Midori-2	2002	No	807.7	98.30	3680	0.000141	0.010003	2	1
70	38771	Metop-B	2012	Yes	824.7	98.73	4090	0.000101	0.001418	3	36
69	29499	Metop-A	2006	No	824.6	98.67	4090	0.000101	0.008641	4	2
178	20322	COBE	1989	No	882.5	99.00	2250	6.25E-05	0.008329	18	4

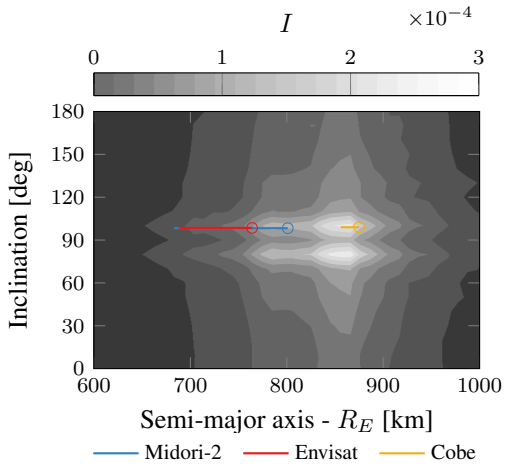

Figure 11. Evolution of the trajectories of the three objects on the map of I. The circle indicates the initial condition.

the other satellites (including Metop-A[2]) are considered not active, so the change of I in time is only due to the evolution of the trajectory. In particular, the comparison between Metop-A and Metop-B is useful to understand how the disposal largely reduces the cumulative value of the index, which for Metop-B is around 16% of the value of Metop-A.

It is also interesting to observe how I evolves along the mission profiles for the three inactive satellites shown in Fig. 11. In particular, I decreases for Envisat, it is almost constant for Midori-2, and it increases for COBE. The reason for these behaviours can be easily explained by looking at Fig. 11, which shows the evolution of the three trajectories, superimposed on the map of the variation of I with the orbital parameters. One can see how Envisat, beginning at the lowest altitude of the three objects, is the one that experiences the largest variation in the semi-major axis and it leaves the most critical region. Conversely, the evolution of the trajectory of COBE moves it to the peak of I.

The graph in Fig. 10 shows that the computation of the index along a mission profile is feasible and gives results in line with the expectations that a spacecraft that do not adopt an end-of-life strategy has a higher impact on the environment compared to one that is compliant with current guidelines. On the other hand, the application of this approach to the whole population within a database can pose some questions. In fact, an automatic definition of disposal strategies is required when thousands of objects are analysed as in the case of the DISCOS population, which contains spacecraft information (e.g. size, mass, year of launch, orbit) for all trackable, unclassified objects. This can introduce a high level of arbitrariness, considering that it is not straightforward to identify which objects are operational and what is the current level of adoption of disposal strategies [6]. The analysis in Fig. 10 could be instead suitable to compare different disposal strategies for the same spacecraft, as shown in Fig. 12. The graph compares the evolution of the index for a spacecraft with mass equal to $80\,\mathrm{kg}$, in orbit at $750\,\mathrm{km}$ altitude, with inclination equal to 98°. For all cases, an operational lifetime equal to ten years is considered, after which three possible disposal strategies are simulated. In the first case, no disposal is performed: as a result, after 90 years from the end of mission, the spacecraft is still in orbit at an altitude slightly lower than $700\,\mathrm{km}$. In the second case, the spacecraft is moved to an orbit with altitude equal to $600\,\mathrm{km}$, from where the spacecraft re-enters in the atmosphere within 20 years from the end of mission. In the third case, at the end of mission a drag sail with cross-sectional area equal to $2\,\mathrm{m}^2$ is deployed. The values chosen for the mass and the sail area replicate those of the sail Icarus 3 developed for the satellite Carbonite [8], which is in orbit at a much lower altitude than the value of $750\,\mathrm{km}$ used for this test. Thanks to the deployment of the sail, the re-entry from the orbit at $750\,\mathrm{km}$ occurs in around 30 years.

To correctly consider the collision probability for the sail it should be considered that p_c represents the probability of catastrophic collisions only. This means that it would not be correct to consider the whole sail area in the computation of the collision probability. Visagie et al. [19] have shown that different parts of a sail experience different effects following a collision. According to their analysis, collisions with a thin membrane do not generate a large number of additional fragments, differently from impacts with the satellite bus and with the sail booms. Following this observation, they suggest the definition of the so-called *debris-generating* cross-sectional area. The case of a square sail with four booms is considered and the same geometry is used also in the present work. For the current analysis, the impactor size is set equal to

[2] which is actually still active; note that only a simple criterion based on the year of launch was used for this analysis. This was done because the purpose was only to demonstrate the feasibility of the computation of the index for a catalogue of space objects, assuming standard disposal behaviours.

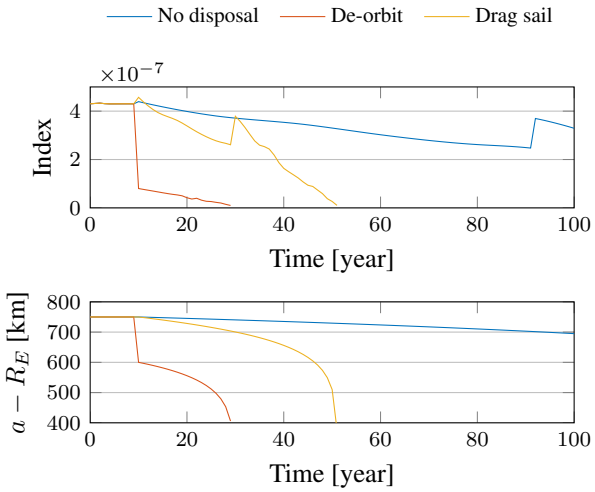

Figure 12. Index and semi-major axis evolution for different disposal options applying a correcting factor to the collisional area of the drag sail.

$r_{\text{debris}} = 1\,\text{cm}$.

As a result, the cross-sectional area used for the computation of the collision probability is equal to $0.5\,\text{m}^2$ instead of the full section of the sail. Fig. 12 shows how the use of the sail appears advantageous from the point of view of the environmental index, with a cumulative index equal to 3.44×10^{-5} for the case with no disposal and 1.51×10^{-5} for the case with the sail.

5. APPLICATION TO CONSTELLATIONS

In recent years, several constellation projects have been proposed. Some of these constellations are composed of hundreds of satellites, so the term *mega-constellations* was introduced. Some preliminary analyses of the impact of those constellations on the debris environment was carried out by [18, 14]. In this Section, it is discussed how the index can be computed when dealing with constellations instead of single objects. The constellation used for this example is Iridium Next, which will be formed by 66 satellites in orbit at $780\,\text{km}$ of altitude[3] and whose first ten satellites were launched at the beginning of this year[4]. The parameters for the constellations are reported in Tab. 4; an area-to-mass ratio $A/M = 0.01\,\text{m}^2\,\text{kg}^{-1}$ is used. This constellation was chosen because its altitude and inclinations are close to the most critical orbital regions according to the proposed index formulation.

The simplest way to apply the debris index to a constellation is to compute the value of the index for a single spacecraft of the constellation and then multiply it by the number of satellites in the constellation. The results of this approach are summarised in Tab. 4, where, for the sake of simplicity, only the part relative to collisions (I_c) is considered and the index is computed at a single epoch, even if the same approach to treat missions profiles is applicable also to case of constellations. In the last column in Tab. 4 the value of the index is normalised to the value of the index of Envisat, so that one can immediately assess the effect of the constellations.

Tab. 4 shows that the value of the index for the single satellites is much smaller than the value for Envisat, but when the whole constellation is considered the reference value is reached and exceeded. This suggests that, according to this simplified model where we consider the value of the index only at a fixed epoch, a constellation such as Iridium Next has a far larger impact on the debris environment than the most critical spacecraft already in orbit.

It is also interesting to observe the value of the cumulative mass and cross-sectional area for the constellation. For example, the value for Iridium Next as a whole is around 22% of the total cross-sectional area of operational objects between 400 and $2000\,\text{km}$. This can be clearly seen by looking at the distribution of the cross-sectional area as in Fig. 1, but now including the studied constellation. Fig. 13 shows the resulting distribution. The cell with the grey marker is the one that contains the Iridium Next satellites and it is the one with the highest value of cumulative cross-sectional area. For this reason, one can consider updating the set of reference targets including an additional object to represent the constellation. Given the formulation of the index and how the maps of e_c and e_e are computed, the addition of a new reference object can be managed efficiently. What is needed is to simply compute a new e_c map considering as a target only the new object from the constellation. In other words, for each cell in the grid in semi-major axis and inclination a fragmentation is simulated and the resulting cumulative collision probability for the new object is computed.

When multiple targets are present, the term of the effects is obtained as in Eq. 1

$$e_{c,0} = \sum_{j=1}^{N_T} w_j p_{c,j} \tag{6}$$

and it is useful to recall that the weights w_j are given by the ratio of the cumulative cross-sectional area in the cell $A_{c,j}$ represented by each target over the total value A_0. With the new object (and the addition of the constellation) the new value of e_c is obtained with

$$e_c = \sum_{j=1}^{N_T+1} \tilde{w}_j p_{c,j}, \tag{7}$$

where the weights $\tilde{w}_j$ need to be updated considering that the total cross sectional area has changed by the inclusion of the ara of the constellation (A_{const}).

[3] The parameters for Iridium Next are taken from eoPortal Directory, last access 07/12/2016.

[4] Iridium, Success! The First Ten Iridium NEXT Satellites Have Arrived in Low-Earth Orbit, 14/01/2017.

Table 4. Parameters and index for the example of constellation: (s) indicates values for single satellites, (c) for the whole constellation.

Name	n_{sat}	$a - R_E$ [km]	i [°]	m [kg]	A [m^2]	p_c	e_c	I_c	I_{Env}
Envisat	1	773	98.3	8110	63.0	0.022225	0.007161	1.59E-04	1.00
IridiumNext (s)	1	780	86.4	860	8.6	0.013635	0.001197	1.63E-05	0.10
IridiumNext (c)	66	780	86.4	56760	568	0.899899	0.001197	1.077E-03	6.77

Rearranging Eq. 7, one obtains

$$\begin{aligned} e_c &= \sum_{j=1}^{N_T+1} \tilde{w}_j p_{c,j} \\ &= \sum_{j=1}^{N_T} \frac{A_{c,j}}{A_0 + A_{\text{const}}} p_{c,j} + \frac{A_{\text{const}}}{A_0 + A_{\text{const}}} p_{c,\text{const}} \\ &= \frac{A_0}{A_0 + A_{\text{const}}} \sum_{j=1}^{N_T} \frac{A_{c,j}}{A_0} p_{c,j} + \frac{A_{\text{const}}}{A_0 + A_{\text{const}}} p_{c,\text{const}} \\ &= \frac{A_0}{A_0 + A_{\text{const}}} e_{c,0} + \frac{A_{\text{const}}}{A_0 + A_{\text{const}}} p_{c,\text{const}}, \end{aligned} \tag{8}$$

so all the previous results can be reused and combined with the new map for the constellation only. The generation of the new map requires less than one tenth of the computational time required by the computation of $e_{c,0}$. The same procedure applies also for the term e_e, whereas the probability term are not affected.

For the case of Iridium Next, the updated map is shown in 14. Given that $A_0 = 2594\,\text{m}^2$ and $A_{\text{const}} = 567.6\,\text{m}^2$, the insertion of the constellation has a large impact on the definition of the regions with the highest risk. The top five objects with the highest I_c, whose parameters are listed in Tab. 5, are the same as in the case without constellation, but the relative criticality changes. In particular, the relative criticality of all the objects except ERS-1 is decreased as they are at more distant altitudes from Iridium Next satellites than ERS-1. In addition, and as expected, also the relative criticality of constellation with respect to the value of Envisat increases in the second scenario.

In summary, by modifying the list of reference targets, the environmental impact of a constellation is taken into account also in terms of how their presence affects the definition of risk zones for all objects. This method can also be applied to study the impact of constellations depending on their maintenance strategy (e.g. operational life-time, years allowed for disposal, success of end-of-life manoeuvres).

6. CONCLUSIONS

The debris index ECOB was extended both in applicability and scope. The present work focussed on the second aspect; in particular, the new formulation of the index was described. The index is composed by two terms that quantify the potential effect of the fragmentation of the

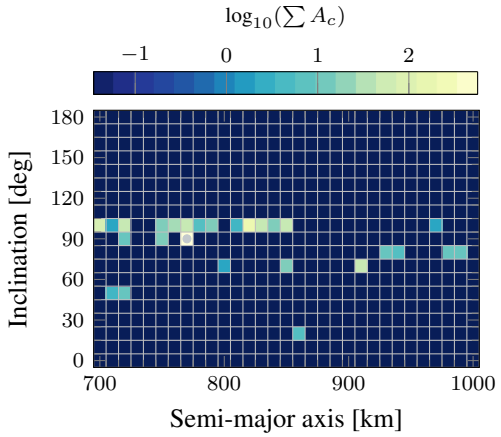

Figure 13. Distribution of the cross-sectional area of spacecraft launched in the last 10 years, in orbit between 700 and 1000 km, plus the Iridium Next constellation.

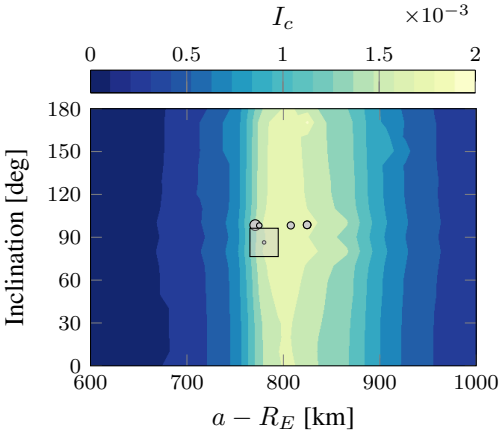

Figure 14. Top five payloads with the highest I_c when Iridium Next is considered. The square indicates the constellation.

Table 5. Top five payloads with the highest I_c when Iridium Next is considered. The number in parentheses indicates the normalised value of the index when the constellation is not included in the reference targets.

SATNO	Name	$a - R_E$ [km]	i [°]	m [kg]	A [m^2]	p_c	e_c	I_c	I_{Env}
27386	Envisat	770.8	98.5	8110	63.0	0.022225	0.062432	0.001388	1.00 (1.00)
27597	Midori-2	807.7	98.3	3680	55.6	0.029950	0.042619	0.001276	0.92 (0.89)
38771	Metop-B	824.7	98.7	4090	37.5	0.017643	0.043488	0.000767	0.55 (0.64)
29499	Metop-A	824.6	98.7	4090	37.5	0.017629	0.043502	0.000767	0.55 (0.64)
21574	ERS-1	775.0	98.2	2140	19.3	0.027819	0.024098	0.000670	0.48 (0.48)
-	IridiumNext (s)	780.0	86.4	860	8.6	0.013635	0.012583	0.000172	0.12 (0.10)
-	IridiumNext (c)	780.0	86.4	56760	567.6	0.899899	0.012583	0.011323	8.16 (6.77)

studied space object, distinguishing between the case of collisions and explosions. Further two terms estimate the probability that these fragmentations occur. As in ECOB, the effect of fragmentation is measured by the resulting increase in the collision probability for operational satellites.

Another point of similarity to ECOB is that the different parts of the index can be evaluated as a function of the considered orbital parameters (i.e. semi-major axis and inclination) and the results for a grid of values can be stored in maps. These maps can then be used to compute the index for specific space objects, without requiring access to any model of space debris evolution.

To distinguish between objects that do and do not adopt end-of-life strategies, the index can be computed along different mission profiles. This was done both to compare different objects in the catalogue and different disposal strategies for the same object. The results of this analysis are affected by the time window adopted for the comparison: a period of 100 years was selected for the current analysis.

Finally, it was shown how the index can be applied to study constellations instead of single objects. A specific effect map for the constellation is generated by adopting as target spacecraft one satellite from the constellation. Then, the effect on the constellation is combined to the previous results related to the other operational spacecraft. This is done by mixing the two effect maps, taking into account how the cumulative cross-sectional area of the constellation compares to the one of the other operational satellites.

ACKNOWLEDGMENTS

Francesca Letizia acknowledges the support from the EPSRC Doctoral Training Partnership at the University of Southampton, grant EP/M508147/1. Francesca Letizia thanks ESA Space Debris Office for the support received during her visiting period in ESOC where part of this work was developed. The authors acknowledge the use of the IRIDIS High Performance Computing Facility, and associated support services at the University of Southampton, in the completion of this work. Data supporting this study are openly available from the University of Southampton repository at http://dx.doi.org/10.5258/SOTON/405121.

REFERENCES

1. Anselmo L. and Pardini C. (2016), Ranking upper stages in low earth orbit for active removal, *Acta Astronautica*, 122:19 – 27.
2. Anselmo L. and Pardini C. (2015), Compliance of the italian satellites in low earth orbit with the end-of-life disposal guidelines for space debris mitigation and ranking of their long-term criticality for the environment, *Acta Astronautica*, 114:93 – 100.
3. Bastida Virgili B. and Krag H. (2013), Active Debris Removal for Leo Missions, In Ouwehand L., editor, *Sixth European Conference on Space Debris*, pages 22–25. ESA Communications, ISBN 978-92-9221-287-2.
4. European Space Agency (2015), ESA Space Debris Mitigation Compliance Verification Guidelines, Technical Report ESSB-HB-U-002, ESA Space Debris Mitigation WG.
5. Flohrer T., Lemmens S., Bastida Virgili B., Krag H., Klinkrad H., Parrilla E., Sanchez N., Oliveira J., and Pina F. (2013), DISCOS - Current status and future developments, In Ouwehand L., editor, *Sixth European Conference on Space Debris*. ESA Communications, ISBN 978-92-9221-287-2.
6. Frey S., Lemmens S., Bastida Virgili B., and Flohrer T. (2016), Level of Adherence to SDM Guidelines, In *Clean Space Industrial Days*.
7. Johnson N. L. and Krisko P. H. (2001), NASA's new breakup model of EVOLVE 4.0, *Advances in Space Research*, 28(9):1377–1384.
8. Kingston J., Palla C., Hobbs S., and Longley J. (2016), Drag-Augmentation System Modules for Small Satellites, In *ESA Clean Space Industry Days*, ESTEC.
9. Letizia F. (2017), Extension of the density approach for debris cloud propagation, Submitted for publication.

10. Letizia F., Colombo C., Lewis H. G., and Krag H. (2016), Assessment of breakup severity on operational satellites, *Advances in Space Research*, 58(7): 1255 – 1274.

11. Letizia F., Colombo C., Lewis H. G., and Krag H. (2016), Development of a debris index, In *Final Stardust Conference*.

12. Lewis H. G., George S. G., Schwarz B. S., and Stokes H., Space debris environment impact rating system.

13. Liou J.-C. and Johnson N. L. (2009), A sensitivity study of the effectiveness of active debris removal in LEO, *Acta Astronautica*, 64(2–3):236–243.

14. Radtke J., Kebschull C., and Stoll E. (2017), Interactions of the space debris environment with mega constellationsusing the example of the oneweb constellation, *Acta Astronautica*, 131:55 – 68.

15. Rossi A., Lewis H. G., White A. E., Anselmo L., Pardini C., Krag H., and Bastida Virigili B. (2015), Analysis of the consequences of fragmentations in Low and Geostationary orbits, *Advances in Space Research*.

16. Rossi A., Valsecchi G. B., and Alessi E. M. (2015), The Criticality of Spacecraft Index, *Advances in Space Research*, 56(3), Special Issue: Advances in Asteroid and Space Debris Science and Technology - Part 1.

17. Utzmann J., Oswald M., Stabroth S., Voigt P., and Retat I. (2012), Ranking and characterization of heavy debris for active removal, In *63rd International Astronautical Congress*. International Astronautical Federation, IAC-12-A6.2.8.

18. Virgili B. B., Dolado J., Lewis H., Radtke J., Krag H., Revelin B., Cazaux C., Colombo C., Crowther R., and Metz M. (2016), Risk to space sustainability from large constellations of satellites, *Acta Astronautica*, 126:154 – 162, Space Flight Safety.

19. Visagie L., Lappas V., and Erb S. (2015), Drag sails for space debris mitigation, *Acta Astronautica*, 109: 65 – 75.

20. Yasaka T. (2011), Can we have an end to the debris issue?, In *62nd International Astronautical Congress*. International Astronautical Federation, IAC-11.A6.5.1.